Unimolecular Decomposition of β-Hydroxyethylperoxy Radicals in the HO•-Initiated Oxidation of Ethene: A Theoretical Study

Santiago Olivella*,† and Albert Solé*,‡

Institut d'Investigacions Químiques i Ambientals de Barcelona, CSIC, Jordi Girona 18, 08034-Barcelona, Catalonia, Spain, and Centre Especial de Recerca en Química Teòrica i Departament de Química Física, Universitat de Barcelona, Martí i Franquès 1, 08028-Barcelona, Catalonia, Spain

Received: September 8, 2004; In Final Form: October 20, 2004

In an attempt to clarify the fate of ethene in the cleaner regions of the troposphere, where the NO_x concentrations are low, the energetical viability of four possible pathways for the unimolecular decomposition of β-hydroxyethylperoxy radical (**1**) have been investigated from the theoretical point of view. The direct hydrogen atom transfer from β-hydroxyethyl radical to triplet O_2 giving either vinyl alcohol or oxirane has also been investigated. Each pathway has been characterized by means of density functional theory (B3LYP) and quantum-mechanical (CCSD(T)) calculations with basis sets ranging in quality from the 6-31G(d,p) to the 6-311+G(3df,2p). The 1,5-migration of the hydroxy H-atom in **1** yielding β-hydroperoxyethoxy radical followed by C−C bond cleavage leading to a hydrogen-bonded [$^{\bullet}CH_2OOH\cdots CH_2O$] complex (CX3) is found to be the energetically preferred pathway. At the RCCSD(T) level of theory, the 0 K energy of the rate-determining transition structure of this mechanism (TS5) is found to lie 3.6 kcal mol^{-1} below the sum of the 0 K energies of the β-hydroxyethyl radical and triplet O_2. Furthermore, it is shown that CX3 can evolve into a three-component hydrogen-bonded [$CH_2O\cdots{}^{\bullet}OH\cdots CH_2O$] complex (CX4) with a 0 K activation energy of only 0.4 kcal mol^{-1}. Assuming that a significant fraction of the β-hydroxyethylperoxy radicals produced in the addition of triplet O_2 to β-hydroxyethyl radical decomposes before collisional stabilization, one might expect the HO•− initiated oxidation of one molecule of ethene to yield two molecules of formaldehyde.

1. Introduction

The oxidation of unsaturated hydrocarbons is an important source of photochemical oxidants in the troposphere. Ethene ($CH_2{=}CH_2$) is among the more abundant unsaturated hydrocarbons emitted both by natural sources (vegetation, soils, and oceans) and by antropogenic sources (burning of biomass and fossil fuels), with a total source strength of about 18−45 Tg/yr.[1,2] The tropospheric oxidation of ethene is initiated primarily by its reaction with the hydroxyl radical (HO•) leading to the formation of the β-hydroxyethyl radical ($^{\bullet}CH_2CH_2OH$).[3]

$$CH_2{=}CH_2 + HO^{\bullet} \rightarrow {}^{\bullet}CH_2CH_2OH \quad (1)$$

The recommended value[4] for the rate coefficient of reaction eq 1 leads to an atmospheric lifetime for ethene of about 1−2 days.[5] The β-hydroxyethyl radical rapidly adds to triplet dioxygen (O_2, $^3\Sigma_g^-$) to form the β-hydroxyethylperoxy radical ($^{\bullet}OOCH_2CH_2OH$).[6,7]

$$^{\bullet}CH_2CH_2OH + O_2 \rightarrow {}^{\bullet}OOCH_2CH_2OH \quad (2)$$

In urban and regionally polluted air, where the nitrogen oxides (NO_x) levels are high, the chemistry of the β-hydroxyethylperoxy radical is dominated by its reaction with nitric oxide ($^{\bullet}NO$) to form β-hydroxyethoxy radical ($^{\bullet}OCH_2CH_2OH$).[7−10]

$$^{\bullet}OOCH_2CH_2OH + {}^{\bullet}NO \rightarrow {}^{\bullet}OCH_2CH_2OH + {}^{\bullet}NO_2 \quad (3)$$

The fate of β-hydroxyethoxy radical is determined by the competition between dissociation (which is dominant) into formaldehyde (CH_2O) and hydroxymethyl radical ($^{\bullet}CH_2OH$) (eq 4) and reaction with triplet O_2 to yield glycolaldehyde ($HOCH_2C(O)H$) and hydroperoxyl radical ($HOO^{\bullet}$) (eq 5).[9,11,12]

$$^{\bullet}OCH_2CH_2OH \rightarrow CH_2O + {}^{\bullet}CH_2OH \quad (4)$$

$$^{\bullet}OCH_2CH_2OH + O_2 \rightarrow HOCH_2C(O)H + HOO^{\bullet} \quad (5)$$

In the upper troposphere, $^{\bullet}NO$ levels are sufficiently high to control the β-hydroxyethylperoxy radical reactivity to yield formaldehyde and glycolaldehyde as major products. In the cleaner regions of the free troposphere and in the marine boundary layer, where the NO_x concentrations are low, other reactions of the β-hydroxyethylperoxy radical will occur, and the fate of ethene in these regions will be different than in polluted regions, where the NO_x levels are high. Since the reaction of triplet O_2 with alkyl radicals leading to the formation of alkylperoxy radicals is always exoergic by 33−37 kcal mol^{-1},[13] the β-hydroxyethylperoxy radical produced in reaction eq 2 is likely to be chemically activated by ∼35 kcal mol^{-1}. This feature suggests that in the absence of $^{\bullet}NO$ one might expect the degradation of β-hydroxyethylperoxy radical to take place through unimolecular reactions with energy barriers below the energy of reactants of reaction eq 2.

* Corresponding author. E-mail: sonqtc@cid.csic.es.
† Institut d'Investigacions Químiques i Ambientals de Barcelona.
‡ Centre Especial de Recerca en Química Teòrica and Departament de Química Física.

10.1021/jp045944f CCC: $27.50 © 2004 American Chemical Society
Published on Web 12/23/2004

In this article we wish to investigate from the theoretical point of view the energetical viability of four possible pathways for the unimolecular decomposition of β-hydroxyethylperoxy radical. The first pathway, labeled as P1, is the concerted elimination of HOO$^\bullet$ from β-hydroxyethylperoxy radical yielding vinyl alcohol (CH_2=CHOH) and HOO$^\bullet$.

$$^\bullet OOCH_2CH_2OH \rightarrow CH_2{=}CHOH + HOO^\bullet \qquad (P1)$$

The second pathway, labeled as P2, is an intramolecular 1,4-hydrogen transfer forming the 1-hydroxy-2-hydroperoxyethyl radical ($^\bullet$CH(OH)CH_2OOH) followed by C−O bond cleavage giving also vinyl alcohol and HOO$^\bullet$.

$$^\bullet OOCH_2CH_2OH \rightarrow {}^\bullet CH(OH)CH_2OOH \rightarrow CH_2{=}CHOH + HOO^\bullet \qquad (P2)$$

The third pathway, labeled as P3, is the same intramolecular 1,4-hydrogen transfer forming the 1-hydroxy-2-hydroperoxyethyl radical but followed by O−O bond cleavage yielding 2-hydroxyoxirane (c-CH_2OCHOH) and HO$^\bullet$.

$$^\bullet OOCH_2CH_2OH \rightarrow {}^\bullet CH(OH)CH_2OOH \rightarrow \text{c-}CH_2OCHOH + HO^\bullet \qquad (P3)$$

The fourth pathway, labeled as P4, is an intramolecular 1,5-hydrogen transfer yielding the β-hydroperoxyethoxy radical (HOO$CH_2CH_2O^\bullet$) followed by C−C bond cleavage leading to hydroperoxymethyl radical ($^\bullet CH_2OOH$) and CH_2O.

$$^\bullet OOCH_2CH_2OH \rightarrow HOOCH_2CH_2O^\bullet \rightarrow {}^\bullet CH_2OOH + CH_2O \qquad (P4)$$

The first step of pathways P2, P3, and P4 are free-radical processes that feature intramolecular abstraction of a hydrogen atom. To compare these intramolecular H-atom abstractions to the closely related direct (bimolecular) H-atom abstraction reactions concerning the $^\bullet CH_2CH_2OH + O_2$ reaction system, we have also investigated the direct β-hydrogen transfer from the β-hydroxyethyl radical to triplet O_2 giving vinyl alcohol and HOO$^\bullet$ (eq 6), as well as the direct hydroxy H-atom transfer from the β-hydroxyethyl radical to triplet O_2 yielding oxirane (c-CH_2CH_2O) and HOO$^\bullet$ (eq 7).

$$^\bullet CH_2CH_2OH + O_2 \rightarrow CH_2{=}CHOH + HOO^\bullet \qquad (6)$$

$$^\bullet CH_2CH_2OH + O_2 \rightarrow \text{c-}CH_2CH_2O + HOO^\bullet \qquad (7)$$

Here we report a complete characterization of 24 stationary points on the ground-state potential energy surface (PES) of the $^\bullet CH_2CH_2OH + O_2$ reaction system, including predictions of geometrical structures, harmonic vibrational frequencies, absolute entropies, and relative energies of minima and transition structures. Energy differences between one-step H-atom transfers and stepwise addition/rearrangement/elimination mechanisms are obtained and rationalized in terms of the structural features shown by the radical intermediates and transition structures involved. As far as we know, this is the first theoretical study on the mechanism of β-hydroxyethyl radical oxidation by triplet O_2 in the gas phase.

2. Computational Methods

The geometries of the relevant stationary points on the ground-state PES of the $^\bullet CH_2CH_2OH + O_2$ reaction system were optimized using analytical gradient procedures,[14] employing density functional theory (DFT) calculations. The spin-unrestricted version of the Becke three-parameter hybrid functional[15] combined with the Lee, Yang, and Parr (LYP) correlation functional,[16] denoted as UB3LYP,[17] was employed with the split-valence 6-31G(d,p) basis set,[18] which includes d-polarization on carbon and oxygen atoms and p-polarization on the hydrogen atoms. All the stationary points were characterized by their harmonic vibrational frequencies as minima or saddle points. Connections of the transition structures between designated minima were confirmed by intrinsic reaction coordinate (IRC)[19] calculations[20] at the UB3LYP/6-31G(d,p) level. All of these calculations were performed with the GAUSSIAN 98 program package.[21]

Since it is well known that the UB3LYP functional underestimates the energy barriers calculated for free-radical H-atom abstraction reactions,[22] we carried out single-point (frozen core) coupled-cluster[23] calculations including all single and double excitations, based on a reference UHF single determinant, together with a perturbative treatment of all connected triple excitations,[24] denoted as UCCSD(T), using the geometries optimized at the UB3LYP/6-31G(d,p) level. Finally, the energies were also evaluated from partially spin-adapted CCSD(T) calculations based on a restricted open-shell Hartree−Fock (ROHF) reference determinant,[25] denoted as RCCSD(T), to accomplish the spin contamination problem in UCCSD(T) wave functions.[26] To establish that our results were converged with respect to basis set, both the UCCSD(T) and RCCSD(T) calculations were carried out with the d,p-polarized split valence 6-311+G(d,p) basis set[27] (which includes a single additional diffuse sp shell[28] on heavy atoms only), with the 6-311+G-(2df,2p) basis set[29] (which includes double d-polarization and a single additional f-polarization on heavy atoms and double p-polarization on hydrogen atoms) and with the 6-311+G-(3df,2p) basis set[29] (which includes triple d-polarization on heavy atoms). The UCCSD(T) calculations were carried out with GAUSSIAN 98, whereas the MOLPRO 98[30] program package was employed for the RCCSD(T) calculations. For comparison purposes, single-point UB3LYP calculations were performed with the 6-311+G(3df,2p) basis set for all the stationary points optimized at the UB3LYP/6-31G(d,p) level.

Zero-point vibrational energies (ZPVEs) were determined from the harmonic vibrational frequencies calculated at the UB3LYP/6-31G(d,p) level. Thermal corrections to enthalpy, absolute entropies, and Gibbs free-energy values were obtained assuming ideal gas behavior from the unscaled harmonic frequencies and moments of inertia by standard methods.[31] A standard pressure of 1 atm was taken in the absolute entropies calculations.

3. Results and Discussion

Selected geometrical parameters of the most relevant stationary points located on the ground-state PES of the $^\bullet CH_2CH_2OH + O_2$ reaction system are shown in Figures 1−5, which are computer-generated plots of the optimized geometries at the UB3LYP level of theory with the 6-31G(d,p) basis set. The Cartesian coordinates of all structures reported in this article are available as Supporting Information. Total energies computed using the UB3LYP functional with the 6-31G(d,p) and 6-311+G(3df,2p) basis sets, as well as the ZPVEs, thermal corrections to enthalpy, and absolute entropies, at the UB3LYP/6-31G(d,p) optimized geometries are collected in Table 1S (Supporting Information). Total energies computed at the UCCSD(T) and RCCSD(T) levels of theory with the 6-311+G-

TABLE 1: Relative Energies (kcal mol^{-1}) Calculated at the B3LYP and RCCSD(T) Levels of Theory with the 6-311+G(3df,2p) Basis Set[a] for Various Species through the $^{\bullet}CH_2CH_2OH + O_2$ Reaction System

	ΔU		ΔE (0 K)		ΔH(298 K)		ΔG(298 K)	
species	B3LYP	RCCSD(T)	B3LYP	RCCSD(T)	B3LYP	RCCSD(T)	B3LYP	RCCSD(T)
$^{\bullet}CH_2CH_2OH + O_2$	0.0	0.0	0.0	0.0	0.0	0.0	0.0	0.0
1	−35.4	−38.7	−29.7	−33.0	−31.3	−34.6	−19.2	−22.5
TS1	−1.2	1.4	−0.4	2.2	−1.7	0.9	10.0	12.6
CX1	−27.5	−27.9	−23.9	−24.3	−24.6	−25.0	−14.3	−14.7
CH_2=CHOH + $^{\bullet}$OO	−21.2	−20.2	−19.7	−18.7	−19.9	−18.9	−19.8	−18.8
TS2	−2.1	−2.7	−0.2	−0.8	−2.0	−2.6	10.7	10.1
2	−23.3	−27.1	−19.4	−23.2	−20.2	−24.0	−9.4	−13.2
TS3	−11.3	−6.7	−8.6	−4.0	−9.4	−4.8	1.1	5.7
TS4	−14.5	−12.2	−12.1	−9.8	−10.6	−10.7	0.3	0.1
CX2	−42.4	−50.0	−39.0	−46.6	−39.9	−47.5	−29.5	−37.1
c-$CH_2OCHOH + ^{\bullet}$OH	−37.5	−43.9	−36.1	−42.5	−36.5	−42.9	−34.1	−40.4
TS5	−12.7	−5.5	−10.8	−3.6	−12.7	−5.5	0.6	7.8
3	−14.9	−16.1	−10.5	−11.7	−12.0	−13.2	0.4	−0.8
TS6	−7.0	−8.1	−5.1	−6.2	−6.1	−7.2	5.2	4.1
CX3	−9.4	−12.3	−8.2	−11.1	−8.1	−11.0	−0.3	−3.2
$^{\bullet}CH_2OOH + CH_2O$	−3.6	−4.6	−4.4	−5.4	−4.1	−5.1	−4.7	−5.7
TS7	−8.9	−10.8	−8.8	−10.7	−8.8	−10.7	−0.9	−2.8
TS8 + CH_2O	−3.7	−3.9	−5.3	−5.5	−5.3	−5.5	−5.5	−5.7
CX4	−41.1	−46.5	−41.7	−47.1	−41.4	−46.8	−35.9	−41.3
$2CH_2O + ^{\bullet}$OH	−33.6	−37.1	−37.6	−41.1	−36.2	−39.7	−45.4	−48.8
TS9	7.8	14.3	7.1	13.6	6.1	12.6	17.2	23.7
TS10	23.7	32.4	23.4	32.1	22.5	31.2	32.7	41.4
CX5	−12.4	−15.4	−8.3	−11.3	−9.1	−12.1	1.2	−1.8
c-$CH_2OCH_2 + ^{\bullet}$OO	−3.3	−4.2	−1.4	−2.3	−1.9	−2.8	−1.2	−2.1

[a] Using the B3LYP/6-31G(d,p) optimized geometries and harmonic vibrational frequencies.

(d,p), 6-311+G(2df,2p), and 6-311+G(3df,2p) basis sets, using the UB3LYP/6-31G(d,p) optimized geometries, are given in Tables 2S and 3S (Supporting Information), respectively. Relative energies calculated at the UB3LYP, UCCSD(T), and RCCSD(T) levels of theory for different basis sets are summarized in Tables 4S−6S (Supporting Information). For all stationary points, Table 1 gives the relative energies (ΔU), as well as the relative energies at 0 K (ΔE(0 K)) and the relative enthalpies (ΔH(298 K)) and Gibbs free energies (ΔG(298 K)) at 298 K, calculated at the UB3LYP/6-311+G(3df,dp) and RCCSD(T)/6-311+G(3df,dp) levels. Finally, Figures 6−8 summarize the 0 K RCCSD(T)/6-311+G(3df,2p) relative energy profiles of the pathways considered in the present study.

3.1. β-Hydroxyethylperoxy Radical. The lowest energy rotational conformer of β-hydroxyethylperoxy radical, labeled as **1**, is shown in Figure 1. In good agreement with UB3LYP calculations with the 6-31G(d) basis set,[32] this conformer has the hydroxy hydrogen atom (H5) pointing directly toward the outer peroxy oxygen atom (O3), with an H···O distance of 2.089 Å. Such geometrical feature indicates that this conformer is energetically stabilized by hydrogen bonding. Table 1 shows that the UB3LYP calculations predict an enthalpy of reaction at 298 K (ΔH_r(298 K)) of −31.3 kcal mol^{-1} for the addition of triplet O_2 to $^{\bullet}CH_2CH_2OH$ leading to **1** (eq 2). This value is greater than the ΔH_r(298 K) of −34.6 kcal mol^{-1} calculated at the RCCSD(T) level of theory for this reaction. Although the experimental ΔH_r(298 K) for reaction eq 2 is unknown, we note that Knyazev and Slagle[33] have obtained an experimental estimate of −35.5 ± 2.0 kcal mol^{-1} for the ΔH_r(298 K) of the addition of triplet O_2 to ethyl radical ($^{\bullet}CH_2CH_3$) leading to ethylperoxy radical ($^{\bullet}OOCH_2CH_3$).

$$^{\bullet}CH_2CH_3 + O_2 \rightarrow {}^{\bullet}OOCH_2CH_3 \qquad (8)$$

By using the geometries and vibrational frequencies computed at the UB3LYP/6-31G(d,p) level for the reactants and product of reaction eq 8, we obtained the values of −30.4 or −33.5 kcal mol^{-1} for the ΔH_r(298 K) of this reaction at the UB3LYP and RCCSD(T) levels of theory, respectively, with the 6-311+G(3df,2p) basis set (see $^{\bullet}OOCH_2CH_3$ in Tables 7S and 8S, Supporting Information). Thus, the RCCSD(T) calculations predict for reaction eq 8 a ΔH_r(298 K) value that is closer to the experimental estimate than to the value afforded by the UB3LYP calculations. Previous theoretical values for the enthalpy of reaction at 0 K reported by Schaefer and coworkers[34] also indicate that the RCCSD(T) method is superior to the UB3LYP functional in the case of reaction eq 8. It is likely, therefore, that the value of the ΔH_r(298 K) provided by the RCCSD(T) calculations for reaction eq 2 is more reliable than the value obtained from the UB3LYP calculations.

3.2. Concerted HOO• Elimination from β-Hydroxyethylperoxy Radical. The transition structure for pathway P1 (see Figure 6), labeled as TS1, is displayed in Figure 1. This transition structure involves the concerted β-hydrogen atom transfer to the outer peroxy oxygen atom and breaking of the C−O bond. It is similar to the transition structure (TS1 therein) calculated by Schaefer and co-workers[34b] at the UB3LYP level with a triple-ζ plus double-polarization plus f functions (TZ2Pf) basis set for the concerted elimination of HOO• from ethylperoxy radical.

$$^{\bullet}OOCH_2CH_3 \rightarrow CH_2{=}CH_2 + HOO^{\bullet} \qquad (9)$$

It is worth noting that the C1−O2−O3−H3−C2 ring in TS1 is nearly planar, the torsion angles C1−O2−O3−H3 and C2−H3−O3−O2 being 1.4 and 14.7°, respectively. These geometrical features suggest that TS1 is not of the conventional radical hydrogen abstraction type. To illustrate this point, Scheme 1 shows a diagrammatic representation of the electronic structure of the reactant, transition structure, and product for the concerted HOO• elimination from β-hydroxyethylperoxy radical through TS1. For simplicity we assume that the C1−C2, C1−O2, O2−O3, and C2−H3 bonds in β-hydroxyethylperoxy radical lie in the plane of the paper. Following the convention of Goddard et al.,[35] we have ignored the core orbitals, 1s for carbon, 1s and 2s for oxygen, which are tightly

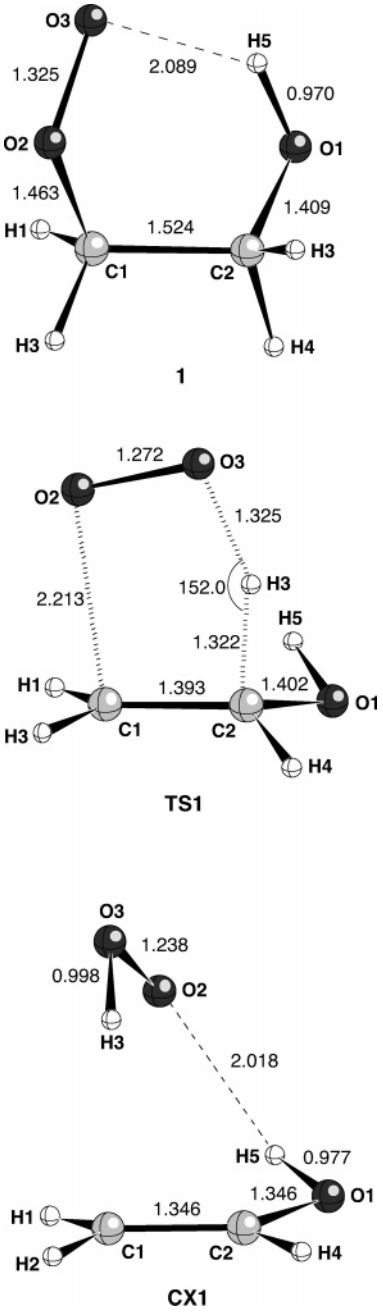

Figure 1. Selected geometrical parameters of the UB3LYP/6-31G-(d,p)-optimized geometries of the equilibrium structure for the β-hydroxyethylperoxy radical (**1**), the transition structure (TS1) for the concerted HOO$^{\bullet}$ elimination from **1**, and the equilibrium structure for the hydrogen-bonded complex (CX1) between vinyl alcohol and HOO$^{\bullet}$. Distances are given in Å and angles in deg.

bound and remain relatively unchanged as the atoms are brought together to form the molecules. The 1s orbital of the migrating hydrogen atom (H3) is represented by a thin circle and the carbon and oxygen 2p orbitals perpendicular to the plane of the paper are each represented by heavy circles. Dots indicate the number of electrons in each orbital, tie lines indicate the coupling of two singly occupied orbitals into a bonding pair. The curved arrows represent actual movement of both covalent and unshared electron pairs, and the curved semiarrow represents actual movement of a single electron along the reaction path. The dramatic qualitative difference between TS1 and the transition structures of free-radical hydrogen abstractions is that the single occupied molecular orbital (SOMO) in TS1 is nearly

SCHEME 1: Diagrammatic Representation of the Electronic Structure of the Reactant, Transition Structure, and Product for the Concerted HOO$^{\bullet}$ Elimination from β-Hydroxyethylperoxy Radical through TS1

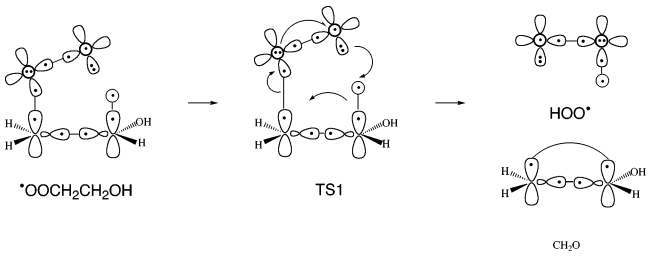

perpendicular to the plane of the paper, while the 1s orbital of the migrating hydrogen lies in this plane. Consequently, in TS1 the SOMO and the latter orbital are nearly orthogonal and their overlap is very small. In other words, the H-atom transfer from the C−H bond to the outer peroxy oxygen cannot take place through an internal free-radical H-atom abstraction. From a qualitative point of view, the primary changes in bonding occurring in TS1 can be described as a formal shift of the unshared electron pair on the terminal oxygen (O3) to the hydrogen atom being transferred (H3) with the simultaneous shift of the electron pair of the C2−H3 bond to the adjacent carbon atom (C1) and the shift of the electron pair of the C1−O2 bond to the oxygen atom (O2). The odd-electron is initially in the 2p orbital of the terminal oxygen (O3) that is perpendicular to the plane of the paper and ends up in the 2p orbital of the adjacent oxygen (O2) that is also perpendicular to the same plane. During the course of the reaction, a proton and a single electron are transferred simultaneously from the CH_2-CH_2OH moiety to the terminal oxygen of the peroxy group, (O3). These electronic features indicate that the mechanism of the H-atom transfer in β-hydroxyethylperoxy radical leading to the concerted HOO$^{\bullet}$ elimination through TS1 is an internal proton-coupled electron-transfer type rather than an intramolecular free-radical H-atom abstraction.[36]

The ΔE(0 K) data listed in Table 1 show that the concerted HOO$^{\bullet}$ elimination from **1** through TS1 involves a 0 K activation energy ($\Delta E^{\ddagger}$ (0 K)) of 29.3 (UB3LYP) or 35.2 (RCCSD(T)) kcal mol^{-1}. Since **1** is found to lie 29.7 (UB3LYP) or 33.0 (RCCSD(T)) kcal mol^{-1} below the sum of the energies of $^{\bullet}CH_2CH_2OH$ and O_2, it follows that, when formed from reaction eq 2, **1** contains an excess of energy which is stored in vibrations and rotations. It is likely that the UB3LYP calculated energy excess of **1** (29.7 kcal mol^{-1}) suffices for overcoming, to some extent, the activation energy of 29.3 kcal mol^{-1} found for the concerted HOO$^{\bullet}$ elimination from **1** through TS1, while the RCCSD(T) calculated energy excess of **1** (33.0 kcal mol^{-1}) does not suffice for surmounting the corresponding activation energy barrier of 35.2 kcal mol^{-1}.

To investigate the effect of substituting a β-hydrogen atom in $^{\bullet}OOCH_2CH_3$ by the HO group on the $\Delta E^{\ddagger}$(0 K) calculated for the concerted elimination of HOO$^{\bullet}$, we computed for reaction eq 9 the activation energy of such pathway by using the geometries and vibrational frequencies of the reactant and transition structure optimized at the UB3LYP/6-31G(d,p) level and the energies calculated at the UB3LYP and RCCSD(T) levels of theory with the 6-311+G(3df,2p) basis set (see $^{\bullet}OOCH_2CH_3$ and TS1′ in Tables 7S and 8S, Supporting Information). The UB3LYP and RCCSD(T) calculations afford the values of 27.3 and 32.6 kcal mol^{-1}, respectively, for the $\Delta E^{\ddagger}$ (0 K) of reaction eq 9, which are in reasonable agreement

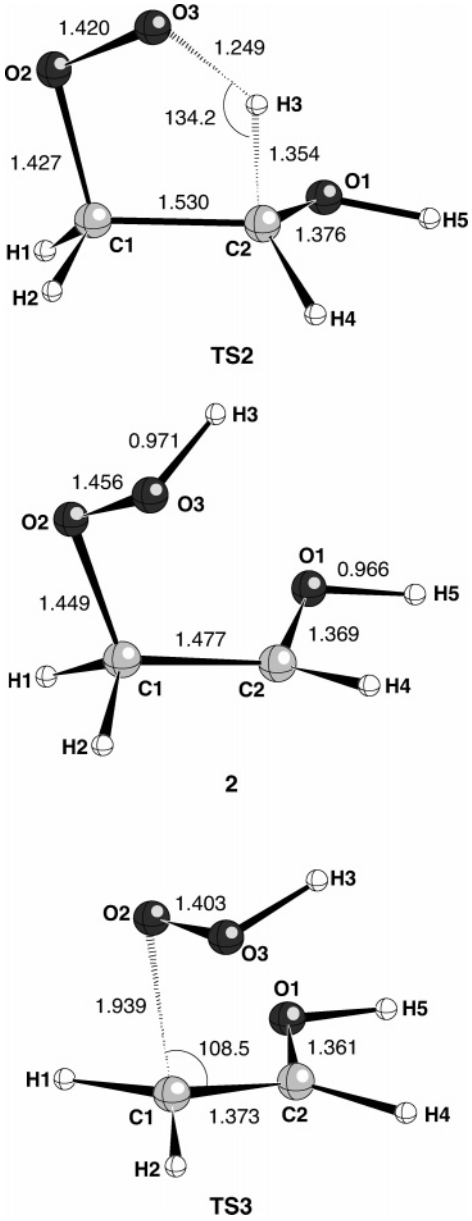

Figure 2. Selected geometrical parameters of the UB3LYP/6-31G-(d,p)-optimized geometries of the transition structure (TS2) for the β-hydrogen atom transfer to the outer peroxy oxygen atom in β-hydroxyethylperoxy radical, the equilibrium structure for the 1-hydroxy-2-hydroperoxyethyl radical (**2**), and the transition structure (TS3) for the HOO$^\bullet$ elimination from **2**. Distances are given in Å and angles in deg.

with the values reported by Schaefer and co-workers for the same reaction. Thus, using the UB3LYP functional with a TZ2Pf basis set to optimize the geometries and a double-ζ plus polarization (DZP) basis set to compute the vibrational frequencies, Ignatyev, Xie, Allen, and Schaefer[34b] found a $\Delta E^{\ddagger}$ (0 K) of 27.1 kcal mol^{-1}, while employing the RCCSD(T) method with a triple-ζ plus double-polarization (TZ2P) basis set (using RCCSD(T)/DZP optimized geometries and CCSD/DZP vibrational frequencies), Rienstra-Kiracofe, Allen, and Schaefer[34a] found a $\Delta E^{\ddagger}$ (0 K) of 30.5 kcal mo1^{-1}. According to our calculations, it appears that the substitution of a β-hydrogen atom in $^\bullet$OOCH$_2$CH$_3$ by the HO group increases the $\Delta E^{\ddagger}$ (0 K) for the concerted elimination of HOO$^\bullet$ by 2.0 (UB3LYP) or 2.6 (RCCSD(T)) kcal mol^{-1}.

The IRC calculations showed that TS1 goes backward to the β-hydroxyethylperoxy radical **1** and goes forward to give a hydrogen-bonded [CH$_2$═CHOH···HOO$^\bullet$] complex. The optimized geometry of this complex, labeled as CX1 (Figure 1), was characterized as a true local minimum on the PES. The ΔU data listed in Table 1 show that CX1 lies 6.3 (UB3LYP) or 7.7 (RCCSD(T)) kcal mol^{-1} below the energy of the isolated products CH$_2$═CHOH and HOO$^\bullet$. Inclusion of the correction for the basis set superposition effects (BSSE), calculated by using the counterpoise method,[37,38] leads to a stabilization energy of CX1 toward decomposition into CH$_2$═CHOH plus HOO$^\bullet$ of 6.2 kcal mol^{-1} at the RCCSD(T) level of theory with the 6-311+G(3df,2p) basis set. After addition of the ZPVE correction, this stabilization energy is reduced to 4.1 kcal mol^{-1}. We did not find an energetic barrier other than that imposed by the endoergicity for the CX1 complex to break apart to form CH$_2$═CHOH plus HOO$^\bullet$.

SCHEME 2: Diagrammatic Representation of the Electronic Structure of the Reactant, Transition Structure, and Product for the Rearrangement of β-Hydroxyethylperoxy Radical to 1-Hydroxy-2-hydroperoxyethyl Radical through TS2

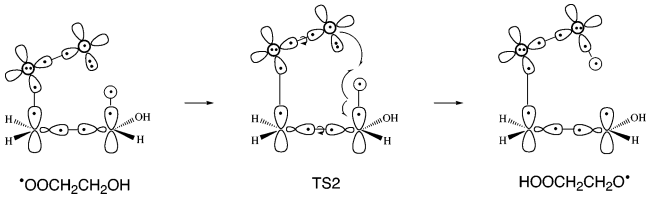

Although pathway P1 is predicted to be endoergic with a calculated 0 K energy of reaction (ΔE_r(0 K)) of 10.0 (UB3LYP) or 14.3 (RCCSD(T)) kcal mol^{-1} (see Table 1), it is interesting to note that the overall oxidation of $^\bullet$CH$_2$CH$_2$OH by O$_2$ yielding CH$_2$═CHOH plus HOO$^\bullet$ is predicted to be an exoergic process with a calculated ΔE_r(0 K) of −19.7 (UB3LYP) or −18.7 (RCCSD(T)) kcal mol^{-1}.

3.3. 1,4-Hydrogen Transfer in β-Hydroxyethylperoxy Radical with C−O Bond Cleavage. The first step of reaction pathway P2 (see Figure 6) is the formation of the 1-hydroxy-2-hydroperoxyethyl radical intermediate by internal β-hydrogen atom transfer to the outer peroxy oxygen atom in the β-hydroxyethylperoxy radical. The optimized geometries of the transition structure for this intramolecular 1,4-hydrogen shift, labeled as TS2, is shown in Figure 2. TS2 is similar to the transition structure (TS2 therein) calculated by Schaefer and co-workers[34b] at the UB3LYP level with a TZ2Pf basis set for the 1,4-hydrogen shift in ethylperoxy radical leading to β-hydroperoxyethyl radical ($^\bullet$CH$_2$CH$_2$OOH).

$$^\bullet\text{OOCH}_2\text{CH}_3 \rightarrow {}^\bullet\text{CH}_2\text{CH}_2\text{OOH} \qquad (10)$$

In contrast to the nearly planar geometry of the C1−O2−O3−H3−C2 ring in TS1, this ring shows a puckered geometry in TS2, with torsion angles C1−O2−O3−H3 and C2−H3−O3−O2 of 35.8° and −22.1°, respectively. This puckering allows the overlap between the 1s orbital of the migrating hydrogen atom (H3) and the singly occupied 2p orbital of the outer peroxy oxygen atom (O3). From the electronic structure point of view, TS2 is a transition structure of the conventional H-atom abstraction by radicals type. A diagrammatic representation of the electronic structure of the reactant, transition structure, and product for the rearrangement of β-hydroxyethylperoxy radical to 1-hydroxy-2-hydroperoxyethyl radical through TS2 is displayed in Scheme 2, where the curved semiarrows represent actual movement of single electrons along the reaction path.

The equilibrium structure of the 1-hydroxy-2-hydroperoxyethyl radical intermediate, labeled as **2**, is shown in Figure 2. The ΔE(0 K) data given in Table 1 show that the 1,4-hydrogen shift in **1** to yield **2** is endoergic, with a calculated ΔE_r(0 K) of 10.3 (UB3LYP) or 9.8 (RCCSD(T)) kcal mol^{-1}, and involves a $\Delta E^{\ddagger}$ (0 K) of 29.5 (UB3LYP) or 32.2 (RCCSD(T)) kcal mol^{-1}. As noted above, when formed from reaction eq 2, **1** contains an energy excess of 29.7 (UB3LYP) or 33.0 (RCCSD(T)) kcal mol^{-1}, which is stored in vibrations and rotations. Therefore, both the UB3LYP and RCCSD(T) calculations predict that the energy excess of **1** might suffice for overcoming, to a certain extent, the energy barrier found for the 1,4-hydrogen shift in **1** to afford **2**.

To investigate the effect of the substitution of a β-hydrogen atom in ethylperoxy radical by the HO group on the $\Delta E^{\ddagger}$ (0 K) for the 1,4-hydrogen shift, we computed the activation energy of reaction eq 10 by using the geometries and vibrational frequencies of the reactant and the transition structure optimized at the UB3LYP/6-31G(d,p) level and the energies calculated at the UB3LYP and RCCSD(T) levels of theory with the 6-311+G-(3df,2p) basis set (see $^{\bullet}OOCH_2CH_3$ and TS2′ in Tables 7S and 8S, Supporting Information). The UB3LYP and RCCSD(T) calculations afford the values of 37.0 and 37.8 kcal mol^{-1}, respectively, for the $\Delta E^{\ddagger}$ (0 K) of reaction eq 10. These values are in good agreement with the $\Delta E^{\ddagger}$ (0 K) of 37.0 (UB3LYP/TZ2Pf) and 35.6 (RCCSD(T)/TZ2P) kcal mol^{-1} reported by Schaefer and co-workers for the same reaction.[34a,b] According to our calculations, it appears that such substitution of a β-hydrogen atom in $^{\bullet}OOCH_2CH_3$ by the HO group lowers the $\Delta E^{\ddagger}$ (0 K) for the 1,4-hydrogen shift by 7.5 (UB3LYP) or 5.6 (RCCSD(T)) kcal mol^{-1}.

At this point we note that the relative 0 K energy ordering of TS1 and TS2 predicted by the UB3LYP calculations is at variance with that predicted by the RCCSD(T) calculations. Thus, UB3LYP predicts TS1 to lie 0.2 kcal mol^{-1} below TS2, whereas RCCSD(T) predicts TS1 to lie 3.0 kcal mol^{-1} above TS2 (see Table 1). Nevertheless, both the UB3LYP and RCCSD(T) calculations agree in predicting that the substitution of a β-hydrogen atom in the ethylperoxy radical by the HO group drops the energy gap between the transition structures for the concerted $HOO^{\bullet}$ elimination and the 1,4-hydrogen transfer pathways. In addition, the RCCSD(T) calculations predict that the substitution reverses the relative energy ordering of these transition structures.

The second step of reaction pathway P2 (see Figure 6) is the simple homolytic rupture of the C1−O2 bond in the radical intermediate **2** leading to the CX1 complex, which subsequently breaks apart to form the products CH_2=CHOH + $HOO^{\bullet}$. This step takes place via the transition structure, labeled as TS3, shown in Figure 2. The $\Delta E^{\ddagger}$ (0 K) calculated for this step using the UB3LYP and RCCSD(T) methods, 10.8 and 19.2 kcal mol^{-1} respectively (see Table 1), differ by 8.4 kcal mol^{-1}. However, both methods agree in predicting the energy of TS3 to be lower than that of TS2. Thus, it is the initial barrier to 1-hydroxy-2-hydroperoxyethyl radical formation and not the subsequent $HOO^{\bullet}$ elimination barrier of this intermediate which determines the rate constant for the production of CH_2=CHOH and $HOO^{\bullet}$ from β-hydroxyethylperoxy radical via the stepwise pathway P2.

Assuming that the relative energies provided by the RCCSD-(T) calculations are more reliable than those afforded by the UB3LYP calculations, the main conclusion of this section is that the substitution of a β-hydrogen atom in the ethylperoxy radical by the HO group favors the stepwise over the concerted $HOO^{\bullet}$ elimination.

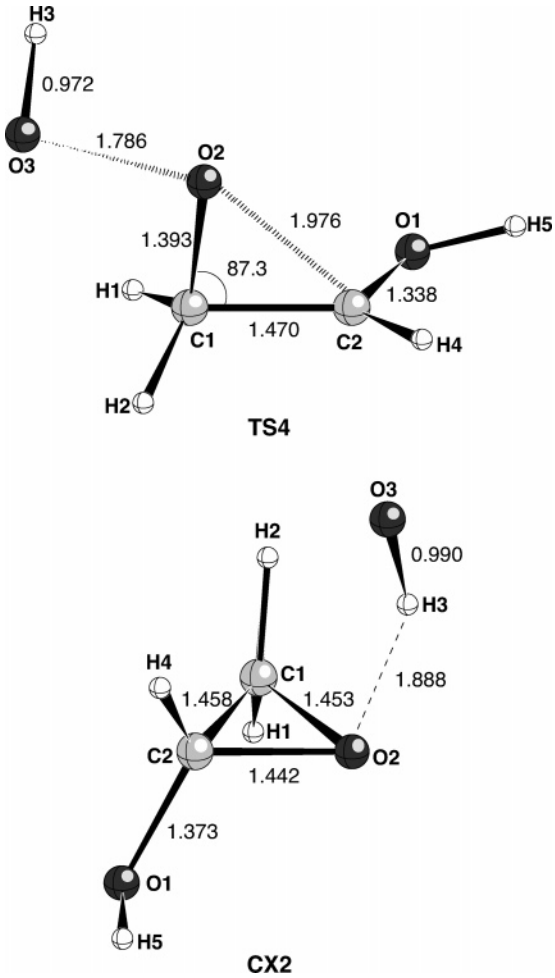

Figure 3. Selected geometrical parameters of the UB3LYP/6-31G-(d,p)-optimized geometries of the transition structure (TS4) for the decomposition of 1-hydroxy-2-hydroperoxyethyl radical and the equilibrium structure for the hydrogen-bonded complex (CX2) between 2-hydroxyoxirane and $HO^{\bullet}$. Distances are given in Å and angles in deg.

3.4. 1,4−Hydrogen Transfer in β-Hydroxyethylperoxy Radical with O−O Bond Rupture. As with mechanism P2, the first step of reaction pathway P3 (see Figure 6) is the formation of the 1-hydroxy-2-hydroperoxyethyl radical by internal β-hydrogen atom transfer to the terminal peroxy oxygen atom in the β-hydroxyethylperoxy radical via TS2. The second step is the decomposition of the 1-hydroxy-2-hydroperoxyethyl radical intermediate into 2-hydroxyoxirane and $HO^{\bullet}$ through O−O bond rupture. The optimized geometry of the transition structure for this decomposition, labeled as TS4, is shown in Figure 3. Note that TS4 involves simultaneous breaking and making of the O2−O3 and C2−O2 bonds, respectively. The $\Delta E^{\ddagger}$ (0 K) calculated for the decomposition of the radical intermediate **2** via TS4, 7.3 (UB3LYP) or 13.4 (RCCSD(T)) kcal mol^{-1}, is 22.2 (UB3LYP) or 18.8 (RCCSD(T)) kcal mol^{-1} lower than the $\Delta E^{\ddagger}$ (0 K) calculated for the initial 1,4-hydrogen shift in the β-hydroxyethylperoxy radical via TS2 (see Table 1). Thus, it is the initial barrier to 1-hydroxy-2-hydroperoxyethyl radical formation and not the subsequent decomposition barrier of such intermediate that determines the rate constant for the production of c-CH_2OCHOH and $HO^{\bullet}$ through pathway P3.

To investigate the effect of substituting a β-hydrogen atom in β-hydroperoxyethyl radical by the HO group on the $\Delta E^{\ddagger}$ (0

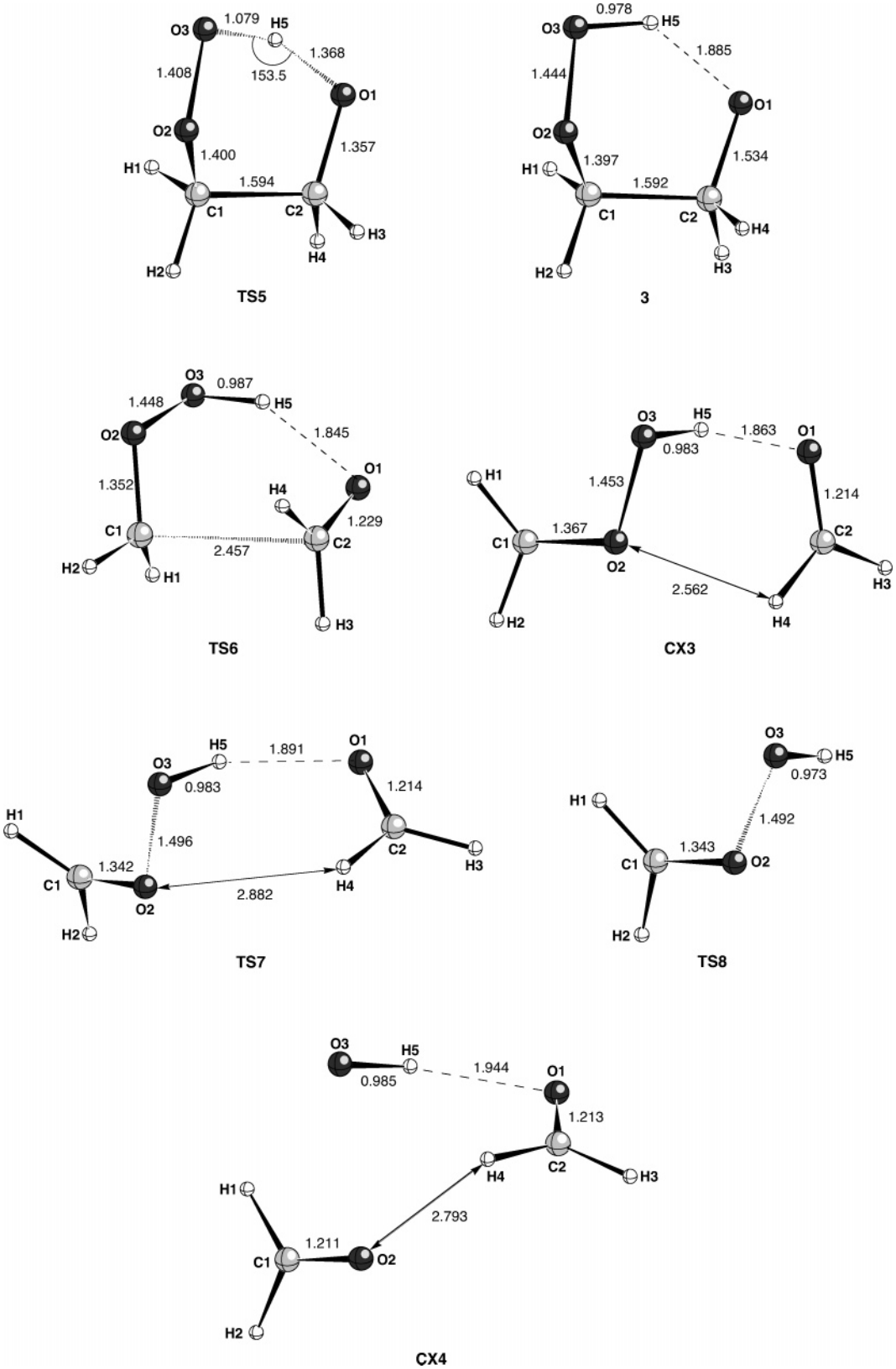

Figure 4. Selected geometrical parameters of the UB3LYP/6-31G(d,p)-optimized geometries of the transition structure (TS5) for the hydroxy hydrogen transfer to the outer peroxy oxygen atom in β-hydroxyethylperoxy radical, the equilibrium structure for the β-hydroperoxyethoxy radical (**3**), the transition structure (TS6) for the CH_2O elimination from **3**, the equilibrium structure for the hydrogen-bonded complex (CX3) between hydroperoxymethyl radical and CH_2O, the transition structure (TS7) for the rupture of the O−O bond within the hydroperoxymethyl unit of CX3, the transition structure (TS8) for the rupture of the O−O bond in hydroperoxymethyl radical, and the hydrogen-bonded complex (CX4) between $HO^{\bullet}$ and two molecules of CH_2O. Distances are given in Å and angles in deg.

K) for its decomposition into oxirane and $HO^{\bullet}$, we computed the activation energy of reaction eq 11 by using the geometries and vibrational frequencies of the reactant and the transition structure optimized at the UB3LYP/6-31G(d,p) level and the energies calculated at the UB3LYP and RCCSD(T) levels with the 6-311+G(3df,2p) basis set (see $^{\bullet}CH_2CH_2OOH$ and TS4′ in

Tables 7S and 8S, Supporting Information).

$$^{\bullet}CH_2CH_2OOH \rightarrow c\text{-}CH_2OCH_2 + HO^{\bullet} \qquad (11)$$

The UB3LYP and RCCSD(T) calculations afford the values of 11.9 and 16.4 kcal mol^{-1}, respectively, for the $\Delta E^{\ddagger}$ (0 K) of reaction eq 11. The latter value is in excellent agreement with the experimental estimate[39] of 16.5 kcal mol^{-1} for the activation energy of reaction eq 11 but 2.5 kcal mol^{-1} higher than the $\Delta E^{\ddagger}$ (0 K) of 13.9 kcal mol^{-1} obtained by Rienstra-Kiracofe, Allen, and Schaefer at the RCCSD(T)/TZ2P level using RCCSD(T)/DZP optimized geometries and CCSD/DZP vibrational frequencies for the same reaction.[34a] According to our calculations, it appears that the substitution of a β-hydrogen atom in β-hydroperoxyethyl radical by the HO group lowers the $\Delta E^{\ddagger}$ (0 K) for its decomposition into oxirane and HO$^{\bullet}$ by 4.6 (UB3LYP) or 3.0 (RCCSD(T)) kcal mol^{-1}.

The IRC calculations showed that TS4 goes backward to the hydroperoxyethyl radical **2** and goes forward to give a hydrogen-bonded [c-$CH_2OCHOH\cdots HO^{\bullet}$] complex. The optimized geometry of this complex, labeled as CX2 (Figure 3), was characterized as a true local minimum on the PES. The ΔU data listed in Table 1 show that CX2 lies 4.9 (UB3LYP) or 6.1 (RCCSD(T)) kcal mol^{-1} below the energy of the isolated products c-CH_2-OCHOH and HO$^{\bullet}$. Inclusion of the correction for the BSSE leads to a stabilization energy of CX2 toward decomposition into c-CH_2OCHOH and HO$^{\bullet}$ of 5.0 kcal mol^{-1} at the RCCSD(T) level of theory with the 6-311+G(3df,2p) basis set. After addition of the ZPVE correction this stabilization energy is reduced to 3.0 kcal mol^{-1}. We did not find an energetic barrier other than that imposed by the endoergicity for the CX2 complex to break apart to form c-CH_2OCHOH and HO$^{\bullet}$.

In contrast to reaction pathway P2, which is predicted to be endoergic with a calculated ΔE_r(0 K) of 10.0 (UB3LYP) or 14.3 (RCCSD(T)) kcal mol^{-1}, pathway P3 is found to be exoergic with a ΔE_r(0 K) of −6.4 (UB3LYP) or −9.5 (RCCSD(T)) kcal mol^{-1} (see Table 1). However, it is likely that the reaction pathways P2 and P3 take place at comparable rates because, as indicated above, TS2 determines the rate constant in both pathways.

3.5. 1,5-Hydrogen Transfer in β-Hydroxyethylperoxy Radical with C−C Bond Rupture. The first step of reaction pathway P4 (see Figure 7) is the formation of a β-hydroperoxyethoxy radical intermediate by internal hydroxy H-atom transfer to the outer peroxy oxygen atom in the β-hydroxyethylperoxy radical. The optimized geometries of the transition structure for this intramolecular 1,5-hydrogen shift, labeled as TS5, is shown in Figure 4. From the geometrical point of view, it is interesting to note that the C1−O2−O3−H5−O1−C2 ring in TS5 is puckered, with torsion angles C1−O2−O3−H5, C2−O1−H5−O3, and C2−C1−O2−O3 of −49.2, −19.5, and 68.3°, respectively. This ring puckering allows the overlap between the 1s orbital of the migrating hydrogen atom (H5) and the singly occupied 2p orbital of the outer peroxy oxygen atom (O3). As in the case of TS2, TS5 is a transition structure of the conventional hydrogen abstraction by radicals type.

The equilibrium structure of the β-hydroperoxyethoxy radical resulting from the intramolecular 1,5-hydrogen shift in the β-hydroxyethylperoxy radical, labeled as **3**, is shown in Figure 4. This conformer has the hydroxy hydrogen atom (H5) pointing directly toward the ethoxy oxygen atom (O1), with an H···O distance of 1.885 Å. Such geometrical feature indicates that this conformer is energetically stabilized by hydrogen bonding. Interestingly, hydroperoxide **3** is found to be more energetic than the isomeric hydroperoxide **2** (see Table 1). This feature can be traced to the expected lower energy of the α-hydroxyethyl radical as compared to the ethoxy radical.[40] As a consequence, the ΔE_r(0 K) calculated for the rearrangement of **1** to **3**, 19.2 (UB3LYP) or 21.3 (RCCSD(T)) kcal mol^{-1}, is about twice the value of 10.3 (UB3LYP) or 9.8 (RCCSD(T)) kcal mol^{-1} calculated for the rearrangement of **1** to **2**. Nevertheless, in terms of the calculated $\Delta E^{\ddagger}$ (0 K) (see Table 1), the energy barrier for the rearrangement of **1** to **3**, 18.9 (UB3LYP) or 29.4 (RCCSD(T)) kcal mol^{-1}, is lower than the value of 29.5 (UB3LYP) or 32.2 (RCCSD(T)) kcal mol^{-1} for the rearrangement of **1** to **2**. These results can be rationalized in terms of the expected lower strain energy of the six-membered ring of TS5 as compared to the five-membered ring of TS2.

Although the internal 1,5-hydrogen shift in **1** to yield **3** via TS5 involves a substantial energy barrier, it is worth noting that, in terms of the calculated 0 K energies, such transition structure lies 10.8 (UB3LYP) or 3.6 (RCCSD(T)) kcal mol^{-1} below $^{\bullet}CH_2CH_2OH$ plus O_2 (see Table 1). Therefore, both the UB3LYP and RCCSD(T) calculations predict that the energy excess of **1** stored in vibrations and rotations might suffice for overcoming, to a certain extent, the activation energy barrier found for the 1,5-hydrogen shift in **1** to afford **3**.

The second step of reaction pathway P4 (see Figure 7) is the simple homolytic rupture of the C−C bond in **3** leading to the elimination of formaldehyde. This step takes place via the transition structure, labeled as TS6, displayed in Figure 4 with a calculated $\Delta E^{\ddagger}$ (0 K) of 5.4 (UB3LYP) or 5.5 (RCCSD(T)) kcal mol^{-1}. On the basis of the ΔE(0 K) data listed in Table 1, we note that the RCCSD(T) calculations predict that TS6 lies 2.6 kcal mol^{-1} below the energy of TS5, while the UB3LYP calculations predict that TS6 lies 5.7 kcal mol^{-1} above the energy of TS5. Assuming that the relative energies provided by the RCCSD(T) method are more reliable than those afforded by the UB3LYP method, it follows that it is the initial barrier to β-hydroperoxyethoxy radical formation and not the subsequent decomposition barrier of this intermediate that determines the rate constant for the production of $^{\bullet}CH_2OOH$ and CH_2O through pathway P4.

The IRC calculations showed that TS6 goes backward to the β-hydroperoxyethoxy radical **3** and goes forward to give a hydrogen-bonded [$^{\bullet}CH_2OOH\cdots OCH_2$] complex. The optimized geometry of this complex, labeled as CX3 (Figure 4), was characterized as a true local minimum on the PES. The ΔU data listed in Table 1 show that CX3 lies 5.8 (UB3LYP) or 7.7 (RCCSD(T)) kcal mol^{-1} below the energy of the isolated components $^{\bullet}CH_2OOH$ and CH_2O. Inclusion of the correction for the BSSE leads to a stabilization energy of CX3 toward decomposition into $^{\bullet}CH_2OOH$ and CH_2O of 6.7 kcal mol^{-1} at the RCCSD(T) level of theory with the 6-311+G(3df,2p) basis set. After addition of the ZPVE correction, this stabilization energy is reduced to 4.7 kcal mol^{-1}. We did not find an energetic barrier other than that imposed by the endoergicity for the CX3 complex to break apart to form $^{\bullet}CH_2OOH$ and CH_2O.

The complex CX3 can evolve by homolytic rupture of the O−O bond of the $^{\bullet}CH_2OOH$ unit, leading to the formation of CH_2O and HO$^{\bullet}$. This process takes place via a low energy transition structure, labeled as TS7, displayed in Figure 4 and involves an energy barrier as low as 0.5 (UB3LYP) or 1.5 (RCCSD(T)) kcal mol^{-1}. After addition of the ZPVE correction, this barrier is reduced to −0.6 (UB3LYP) or 0.4 (RCCSD(T)) kcal mol^{-1}. Interestingly, TS7 is a hydrogen-bonded complex between a molecule of CH_2O and the transition structure for the rupture of the O−O bond in $^{\bullet}CH_2OOH$. To evaluate the stabilization energy of such hydrogen-bonded complex toward

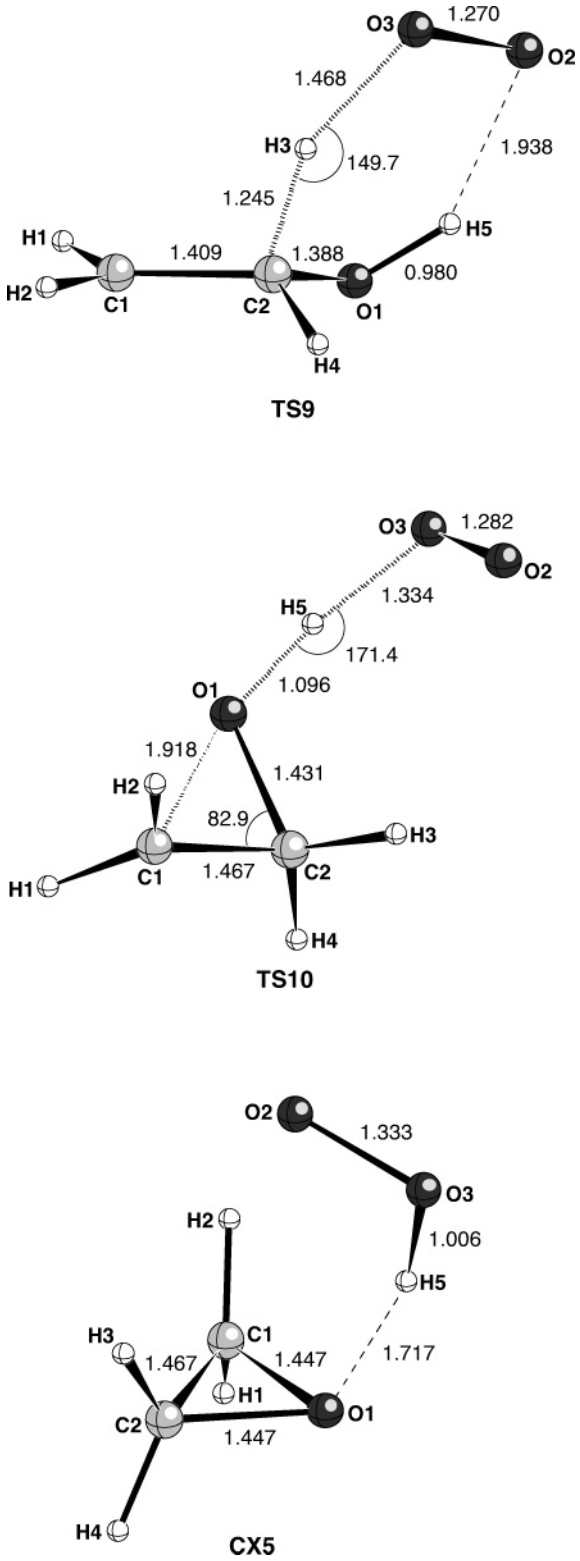

Figure 5. Selected geometrical parameters of the UB3LYP/6-31G-(d,p)-optimized geometry of the transition structure (TS9) for the direct β-hydrogen transfer from β-hydroxyethyl radical to triplet O_2, the transition structure (TS10) for the direct hydroxy hydrogen transfer from β-hydroxyethyl radical to triplet O_2, and the equilibrum structure for the complex (CX5) between oxirane and HOO$^\bullet$. Distances are given in Å and angles in deg.

decomposition into their components, the geometry of the latter transition structure, labeled as TS8, was optimized at the UB3LYP/6-31G(d,p) level. The geometry of TS8 is shown in Figure 4 and the total energies calculated with the UB3LYP, UCCSD(T), and RCCSD(T) methods with the 6-311+G-(3df,2p) basis set are given in Tables 1S−3S (Supporting Information). According to Table 1, TS7 lies 5.2 (UB3LYP) or 6.9 (RCCSD(T)) kcal mol^{-1} below the energy of the isolated components TS8 and CH_2O. Inclusion of the correction for the BSSE leads to a stabilization energy of TS7 toward decomposition into TS8 and CH_2O of 5.9 kcal mol^{-1} at the RCCSD(T) level of theory with the 6-311+G(3df,2p) basis set. After addition of the ZPVE correction this stabilization energy is reduced to 4.2 kcal mol^{-1}.

The IRC calculations showed that TS7 goes backward to the hydrogen-bonded complex CX3 and goes forward to give a three-component hydrogen-bonded [$CH_2O\cdots{}^\bullet OH\cdots OCH_2$] complex. The optimized geometry of this complex, labeled as CX4 (see Figure 4), was characterized as a true local minimum on the PES. The ΔU data listed in Table 1 show that CX4 lies 7.5 (UB3LYP) or 9.4 (RCCSD(T)) kcal mol^{-1} below the energy of the isolated components $2CH_2O$ and HO$^\bullet$. Inclusion of the correction for the BSSE leads to a stabilization energy of CX4 toward decomposition into $2CH_2O$ and HO$^\bullet$ of 7.9 kcal mol^{-1} at the RCCSD(T) level of theory with the 6-311+G(3df,2p) basis set. After addition of the ZPVE correction, this stabilization energy is reduced to 4.5 kcal mol^{-1}. We did not find an energetic barrier other than that imposed by the endoergicity for the CX4 complex to break apart to form $2CH_2O$ and HO$^\bullet$.

At this point we note that the overall decomposition of the β-hydroxyethylperoxy radical yielding formaldehyde and HO$^\bullet$ is exoergic with an ΔE_r(0 K) of −7.9 (UB3LYP) or −8.1-(RCCSD(T)) kcal mol^{-1}. This exoergicity is of the same order of magnitude as the exoergicity calculated for the decomposition of β-hydroxyethylperoxy radical giving 2-hydroxyoxirane and HO$^\bullet$ (i.e., −6.4 (UB3LYP) or −9.5 (RCCSD(T)) kcal mol^{-1}). However, the 0 K energy calculated for the transition structure of the rate-determining step of the former pathway (i.e., TS5) is 10.6 (UB3LYP) or 2.8 (RCCSD(T)) kcal mol^{-1} lower than that calculated for the rate-determining transition structure of the latter pathway (i.e., TS2). Therefore, it follows that the decomposition of the β-hydroxyethylperoxy radical yielding formaldehyde and HO$^\bullet$ is favored over its decomposition giving 2-hydroxyoxirane and HO$^\bullet$.

Assuming that a significant fraction of the β-hydroxyethylperoxy radicals formed in the reaction of β-hydroxyethyl radical with triplet O_2 decompose before collisional stabilization, the preceding results suggest that the HO$^\bullet$-initiated oxidation of ethene might follow the steps outlined in eqs 12a−12e. Note that the HO$^\bullet$ radical initiating the reaction sequence is regenerated so that it can continue the chain reaction.

$$CH_2{=}CH_2 + HO^\bullet \rightarrow {}^\bullet CH_2CH_2OH \quad (12a)$$

$${}^\bullet CH_2CH_2OH + O_2 \rightarrow {}^\bullet OOCH_2CH_2OH \quad (12b)$$

$${}^\bullet OOCH_2CH_2OH \rightarrow HOOCH_2CH_2O^\bullet \quad (12c)$$

$$HOOCH_2CH_2O^\bullet \rightarrow {}^\bullet CH_2OOH + CH_2O \quad (12d)$$

$${}^\bullet CH_2OOH \rightarrow CH_2O + HO^\bullet \quad (12e)$$

Finally, it should be noted that the net result of eqs 12a−12e is the conversion of one molecule of ethene into two molecules of formaldehyde.

$$CH_2{=}CH_2 + O_2 \rightarrow 2CH_2O \quad (13)$$

3.6. Direct β-Hydrogen Transfer from β-Hydroxyethyl Radical to Triplet Dioxygen. The transition structure of the

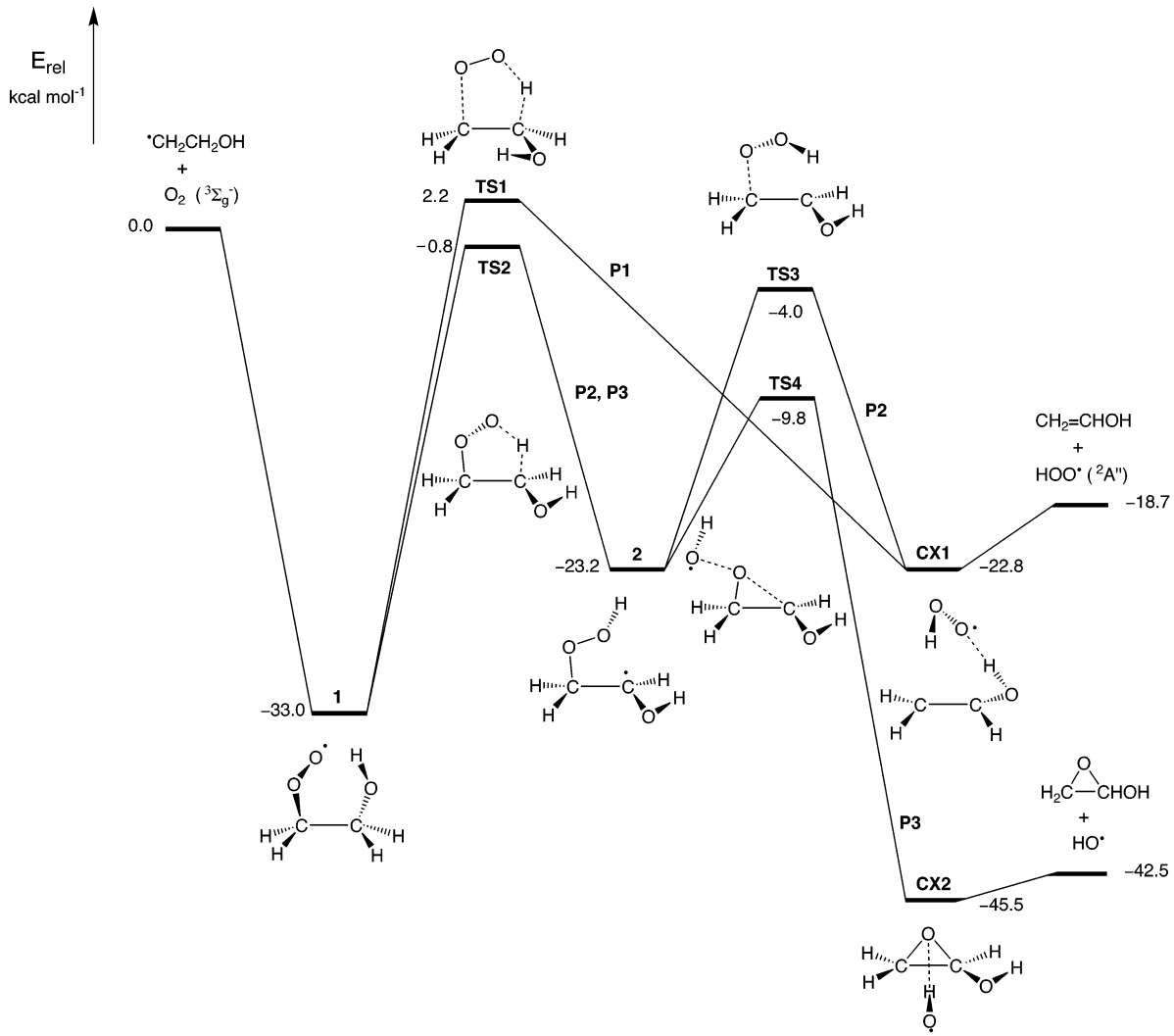

Figure 6. Schematic energy profiles along an arbitrary reaction coordinate showing the structures involved in pathways P1, P2, and P3. Relative energy values obtained from ZPVE-corrected RCCSD(T)/6-311+G(3df,2p) total energies. The BSSE- and ZPVE-corrected total energies were used for the CX1 and CX2 complexes.

one-step β-hydrogen transfer from β-hydroxyethyl radical to triplet O_2 (see eq 6 and Figure 8), labeled as TS9, is displayed in Figure 5. TS9 can be described as the concerted breaking and making of the C2−H3 and O3−H3 bonds, respectively, leading to the formation of the complex CX1. As might be expected, the geometrical parameters of TS9 are very close to those of the transition structure calculated by Ghigo and Tonachini at the UB3LYP level with the 6-31G(d) and 6-311G-(d,p) basis sets for the same reaction.[41] From the geometrical point of view, it is remarkable that TS9 has the hydroxy hydrogen atom (H5) pointing directly toward the outer oxygen atom (O2), with a H···O distance of 1.938 Å. This geometrical feature indicates that such transition structure may be energetically stabilized by hydrogen bonding. To evaluate the effect of such energy stabilization on the barrier for the reaction pathway eq 6, we computed the transition structure of the direct β-hydrogen atom transfer from ethyl radical to triplet O_2

$$\text{•CH}_2\text{CH}_3 + \text{O}_2 \rightarrow \text{CH}_2{=}\text{CH}_2 + \text{HOO•} \qquad (14)$$

The geometry and vibrational frequencies of this transition structure (labeled as TS9′ in Tables 7S and 8S, Supporting Information) were computed at the UB3LYP/6-31G(d,p) level and the energy was evaluated at the UB3LYP and RCCSD(T) levels of theory with the 6-311+G(3df,2p) basis set. Table 1 shows that the direct β-hydrogen transfer from β-hydroxyethyl radical to triplet O_2 (eq 6) via TS9 involves a $\Delta U^{\ddagger}$ of 7.8 (UB3LYP) or 14.3 (RCCSD) kcal mol^{-1}, while Tables 7S and 8S reveal that the direct β-hydrogen atom transfer from ethyl radical to triplet O_2 (eq 14) through TS9′ involves a $\Delta U^{\ddagger}$ of 10.8 (UB3LYP) or 17.3 (RCCSD(T)) kcal mol^{-1}. Therefore, both the UB3LYP and RCCSD(T) calculations indicate that the substitution of a β-hydrogen atom in ethyl radical by the HO group lowers the energy barrier for the direct β-hydrogen transfer to triplet O_2 by 3.0 kcal mol^{-1}. It is likely that the aforementioned hydrogen bond in TS9 accounts for most of this energy barrier lowering.

The energy barrier $\Delta U^{\ddagger}$ of 7.8 kcal mol^{-1} obtained for reaction eq 6 from the UB3LYP/6-311+G(3df,2p) calculations is identical to the barrier reported by Ghigo and Tonachini at the same level of theory using UB3LYP/6-311G(d,p) optimized geometries. In contrast, the RCCSD(T)/6-311+G(3df,2p) calculations afford a $\Delta U^{\ddagger}$ of 14.3 kcal mol^{-1}, which is about twice the energy barrier (7.8 kcal mol^{-1}) obtained from the UB3LYP/6-311+G(3df,2p) calculations. Interestingly, Ghigo and Tonachini obtained a value of 14.5 kcal mol^{-1} for $\Delta U^{\ddagger}$ by using a multireference second-order perturbation theory method based on a complete active space self-consistent field with the 6-311G-(d,p) basis set.[41] To lend further support to our RCCSD(T)/6-

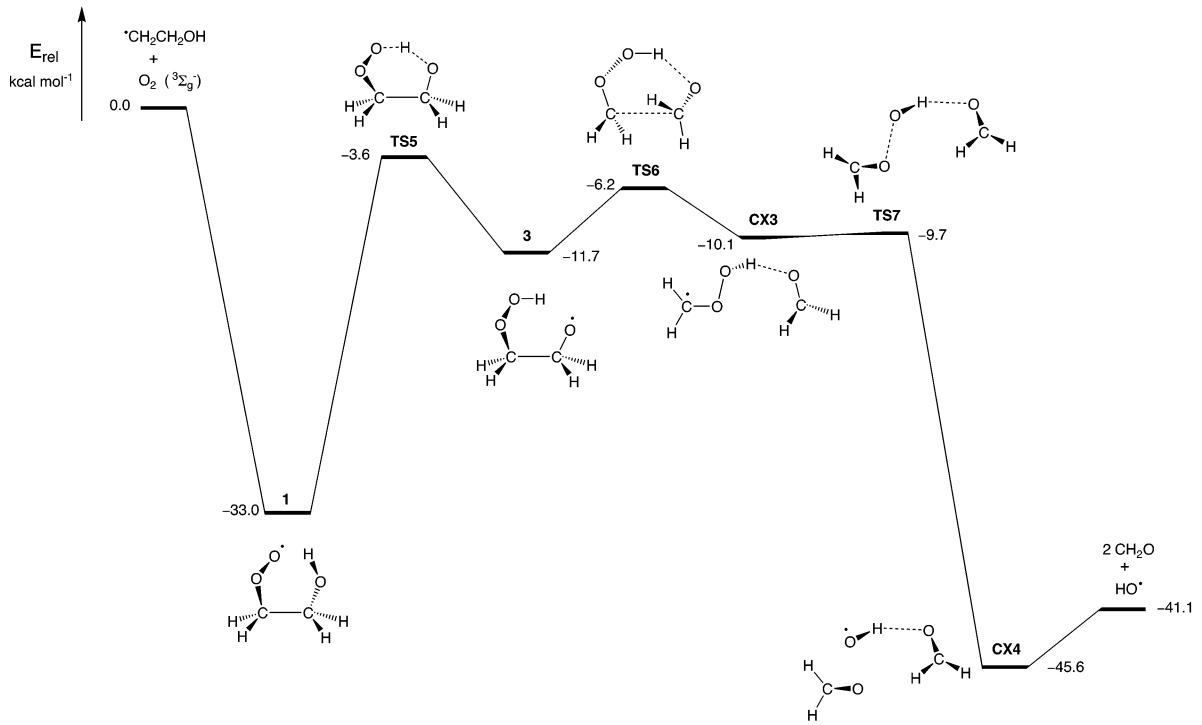

Figure 7. Schematic energy profile along an arbitrary reaction coordinate showing the structures involved in pathway P4. Relative energy values obtained from ZPVE-corrected RCCSD(T)/6-311+G(3df,2p) total energies. The BSSE- and ZPVE-corrected total energies were used for the CX3 and CX4 complexes.

311+G(3df,2p) calculations, we note that at this level of theory the $\Delta U^{\ddagger}$ of reaction eq 14 is found to be 17.3 kcal mol^{-1}, which is in good agreement with the results reported by Schaefer and co-workers for the same reaction. Thus, using RCCSD(T)/TZ2Pf energies evaluated at the RCCSD(T)/TZ2P optimized geometries, Rienstra-Kiracofe, Allen, and Schaefer[34a] found a $\Delta U^{\ddagger}$ of 16.4 kcal mol^{-1} for reaction eq 14. Therefore, it appears that the UB3LYP calculations underestimate significantly the energy barrier of H-atom abstraction reactions by triplet O_2. At any rate, the values of $\Delta E^{\ddagger}$ (0 K) afforded by both the UB3LYP and RCCSD(T) methods (i.e., 7.1 and 13.6 kcal mol^{-1}, respectively) for the one-step mechanism of reaction eq 6 are higher than the values provided by both methods for the same reaction assuming that it takes place through either an addition/elimination mechanism (pathway P1) or an addition/rearrangement/elimination mechanism (pathway P2).

3.7. Direct Hydroxy Hydrogen Transfer from β-Hydroxyethyl Radical to Triplet Dioxygen. The transition structure of the one-step hydroxy hydrogen transfer from β-hydroxyethyl radical to triplet O_2 (see eq 7 and Figure 8), labeled as TS10, is displayed in Figure 5. TS10 involves the concerted breaking of the O1−H5 bond and the making of the O3−H5 and O1−C1 bonds.

The IRC calculations showed that TS10 goes backward to the reactants and goes forward to give a hydrogen-bonded [c-CH_2OCH_2···HOO$^{\bullet}$] complex. The optimized geometry of this complex, labeled as CX5 (Figure 5), was characterized as a true local minimum on the PES. CX5 lies 9.1 (UB3LYP) or 11.2 (RCCSD(T)) kcal mol^{-1} below the energy of the isolated components oxirane and HOO$^{\bullet}$. Inclusion of the correction for the BSSE leads to a stabilization energy of CX5 toward decomposition into their components of 9.6 kcal mol^{-1} at the RCCSD(T) level of theory with the 6-311+G(3df,2p) basis set. After addition of the ZPVE correction, this stabilization energy is reduced to 7.4 kcal mol^{-1}. We did not find an energetic barrier other than that imposed by the endoergicity for the CX5 complex to break apart to form oxirane and HOO$^{\bullet}$.

Table 1 shows that the direct hydroxy hydrogen transfer from β-hydroxyethyl radical to triplet O_2 yielding oxirane and HOO$^{\bullet}$ is slightly exoergic, with a calculated ΔE_r(0 K) of −1.4 (UB3LYP) or −2.3 (RCCSD(T)) kcal mol^{-1}, and involves a substantial $\Delta E^{\ddagger}$ (0 K) of 23.4 (UB3LYP) or 32.1 (RCCSD(T)) kcal mol^{-1}. Taking into account that such reaction is an H-atom abstraction by triplet O_2, the significant difference between the values of $\Delta E^{\ddagger}$ (0 K) provided by the UB3LYP and RCCSD(T) calculations is consistent with the aforementioned tendency of the UB3LYP method to underestimate the energy barriers for such class of H-atom abstractions. In any case, the values of $\Delta E^{\ddagger}$ (0 K) afforded by both the UB3LYP and RCCSD(T) methods for the direct hydroxy hydrogen transfer from β-hydroxyethyl radical to triplet O_2 (eq 7) are much higher than the values predicted by both methods for the competing oxidation of β-hydroxyethyl radical by triplet O_2 leading to the formation of vinyl alcohol (pathways P1, P2, and 6), or 2-hydroxyoxirane (pathway P3), or formaldehyde (pathway P4).

4. Summary and Conclusions

The energetical viability of four hypothetical pathways (P1−P4) for the unimolecular decomposition of β-hydroxyethylperoxy radical, **1**, has been investigated by means of DFT (B3LYP) and quantum-mechanical (CCSD(T)) electronic structure methods. In addition, the one-step hydrogen atom transfers from β-hydroxyethyl radical to triplet O_2 have also been investigated. On the basis of the well know tendency of the B3LYP method to underestimate the energy barriers calculated for free-radical H−atom abstraction reactions, we assume that the RCCSD(T) calculations are more reliable than the B3LYP calculations for the reactions studied in this work. From the analysis of the results of the RCCSD(T) calculations the following main points emerge.

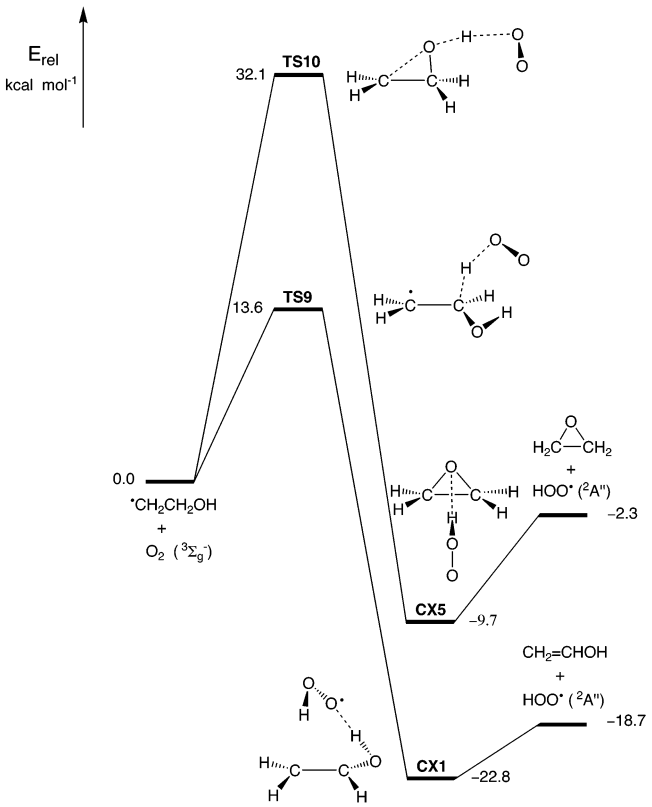

Figure 8. Schematic energy profiles along an arbitrary reaction coordinate showing the structures involved in the direct β-hydrogen transfer from β-hydroxyethyl radical to triplet O_2 and the direct hydroxy hydrogen transfer from β-hydroxyethyl radical to triplet O_2. Relative energy values obtained from ZPVE-corrected RCCSD(T)/6-311+G-(3df,2p) total energies. The BSSE- and ZPVE-corrected total energies were used for the CX1 and CX5 complexes.

(1) The decomposition of **1** affording two molecules of CH_2O and one molecule of HO$^\bullet$, with an overall $\Delta E_r(0\ K)$ of -8.1 kcal mol^{-1}, is the energetically preferred reaction pathway. This pathway (P4) is initiated by the 1,5-hydrogen shift of the hydroxy H-atom to the outer peroxy O-atom to form the β-hydroperoxyethoxy radical, **3**, with a $\Delta E^{\ddagger}$ (0 K) of 29.4 kcal mol^{-1}. Since the transition structure of this step, TS5, lies 3.6 kcal mol^{-1} below the sum of the energies of β-hydroxyethyl radical and triplet O_2, it turns out that when formed from these reactants **1** contains an excess energy which suffices for overcoming such energy barrier. Subsequently, **3** undergoes a C$-$C bond rupture, involving an $\Delta E^{\ddagger}$ (0 K) of 5.5 kcal mol^{-1}, yielding a hydrogen-bonded [$^\bullet$CH$_2$OOH$\cdots$CH$_2$O] complex, CX3. The O$-$O bond cleavage of the $^\bullet$CH$_2$OOH unit of CX3 leads to the formation of a three-component hydrogen-bonded [CH$_2$O$\cdots{}^\bullet$OH$\cdots$CH$_2$O] complex, CX4, with an $\Delta E^{\ddagger}$ (0 K) of only 0.4 kcal mol^{-1}. Finally, CX4 breaks apart yielding 2 CH_2O plus HO$^\bullet$ with an $\Delta E_r(0\ K)$ of 4.5 kcal mol^{-1}.

(2) In clear contrast with the unsubstituted ethylperoxy radical case, the $\Delta E^{\ddagger}$ (0 K) calculated (35.2 kcal mol^{-1}) for the concerted HOO$^\bullet$ elimination from **1**, yielding a hydrogen-bonded [CH$_2$=CHOH$\cdots$HOO$^\bullet$] complex, CX1 (pathway P1), is higher than that calculated (32.2 kcal mol^{-1}) for the stepwise HOO$^\bullet$ elimination via 1,4-hydrogen shift of a β-hydrogen to the outer peroxy O-atom, leading to the 1-hydroxy-2-hydroperoxyethyl radical intermediate, **2**, followed by C$-$O bond cleavage [$\Delta E^{\ddagger}$ (0 K) = 19.2 kcal mol^{-1}] (pathway P2). Intermediate **2** may also undergo O$-$O bond rupture yielding a hydrogen-bonded complex between 2-hydroxyoxirane and HO$^\bullet$, CX2, [$\Delta E^{\ddagger}$ (0 K) = 13.4 kcal mol^{-1}] (pathway P3).

(3) The transition structures of the one-step H-atom transfer from β-hydroxyethyl radical to triplet O_2 giving either vinyl alcohol plus HOO$^\bullet$ or oxirane plus HOO$^\bullet$ are predicted to lie 13.6 and 32.1 kcal mol^{-1}, respectively, above the sum of the 0 K energies of these reactants. Therefore, at the tropospheric temperatures ($\approx$200$-$300 K) such bimolecular reactions cannot compete with the rapid addition of β-hydroxyethyl radical to triplet O_2 forming **1**, followed by its unimolecular decomposition through pathways P1$-$P4.

Assuming that a significant fraction of the β-hydroxyethylperoxy radicals formed in the addition of triplet O_2 to β-hydroxyethyl radical decompose before collisional stabilization, the preceding points suggest that in the cleaner regions of the troposphere, where the NO_x concentrations are low, the HO$^\bullet$$-$initiated oxidation of one molecule of ethene should yield two molecules of CH_2O.

Acknowledgment. This paper is dedicated to Professor Ramon Carbó-Dorca on the occasion of his 65th birthday. This research was supported by the Spanish DGICYT (Grants BQU2002-04485-C02-01 and BQU2002-04485-C02-02). Additional support came from Catalonian CIRIT (Grant 2001SGR00048). The larger calculations described in this work were performed on the CPQ AlphaServer HPC320 at the Centre de Supercomputació de Catalunya (CESCA).

Supporting Information Available: The Cartesian coordinates of all structures reported in this paper, tables summarizing total energies, zero-point vibrational energies, thermal corrections to enthalpy, and absolute entropies. This material is available free of charge via the Internet at http://pubs.acs.org.

References and Notes

(1) Sawada, S.; Totsuka, T. *Atmos. Environ.* **1986**, *20*, 821.
(2) Singh, H. B.; Zimmerman, P. R. Atmospheric distribution and sources of nonmethane hydrocarbons. In. *Gaseous Pollutants: Characterization and Cycling;* Nriagu, J. O., Ed.; John Wiley: New York, 1992; pp 177$-$235.
(3) Atkinson, R. J. *Phys. Chem. Ref. Data* **1997**, *26*, 215.
(4) DeMore, W. B.; Sander, S. P.; Golden, D. M.; Hampson, D. R. F.; Kurylo, M. J.; Howard, C. J.; Ravishankara, A. R.; Kolb, C. E.; Molina, M. J. *Chemical kinetics and photochemical data for use in stratospheric modeling; evaluation number 12;* NASA JPL Publ. No. 97-4; 1997.
(5) Orlando, J. J.; Tyndall, G. S.; Bilde, M.; Ferronato, C.; Wallington, T. J.; Vereecken, L.; Peeters, J. *J. Phys. Chem. A* **1998**, *102*, 8116$-$8123.
(6) Miyoshi, A.; Matsui, H.; Washida, N. *Chem. Phys. Lett.* **1989**, *160*, 291.
(7) Murrells, T. P.; Jenkin, M. E.; Shallinker, S. J.; Hayman, G. D. *J. Chem. Soc., Faraday Trans.* **1991**, *87*, 2351.
(8) Becker, K. H.; Geiger, H.; Wiesen, P. *Chem. Phys. Lett.* **1991**, *184*, 256.
(9) (a) Niki, H.; Maker, P. D.; Savage, C. M.; Breitenbach, L. P. *J. Phys. Chem.* **1978**, *82*, 135. (b) Niki, H.; Maker, P. D.; Savage, C. M.; Breitenbach, L. P. *Chem. Phys. Lett.* **1981**, *80*, 499.
(10) Barnes, I.; Becker, K. H.; Ruppert, L. *Chem. Phys. Lett.* **1993**, *203*, 295.
(11) (a) Atkinson, R.; Carter, W. P. L. *J. Atmos. Chem.* **1991**, *13*, 195. (b) Atkinson, R. *Int. J. Chem. Kinet.* **1997**, *29*, 99.
(12) Dibble, T. S. *Chem. Phys. Lett.* **1999**, *301*, 297$-$302.
(13) Clifford, E. P.; Wenthold, P. G.; Gareyev, R.; Lineberger, W. C. *J. Chem. Phys.* **1998**, *109*, 10293$-$10310.
(14) (a) Schlegel, H. B. *J. Comput. Chem.* **1982**, *3*, 214. (b) Bofill, J. M. *J. Comput. Chem.* **1994**, *15*, 1.
(15) Becke, A. D. *J. Chem. Phys.* **1993**, *98*, 5648.
(16) Lee, C.; Yang, W.; Parr, R. G. *Phys. Rev. B* **1988**, *37*, 785.
(17) Stevens, P. J.; Devlin, F. J.; Chablowski, C. F.; Frisch, M. J. *J. Phys. Chem.* **1994**, *98*, 11623.
(18) Hariharan, C.; Pople, J. A. *Theor. Chim. Acta* **1973**, *28*, 213.
(19) (a) Fukui, K. *Acc. Chem. Res.* **1981**, *14*, 363. (b) Ishida, K.; Morokuma, K.; Kormornicki, A. *J. Chem. Phys.* **1977**, *66*, 2153.

(20) (a) Gonzalez, C.; Schlegel, H. B. *J. Chem. Phys.* **1989**, *90*, 2154. (b) Gonzalez, C.; Schlegel, H. B. *J. Phys. Chem.* **1990**, *94*, 5523.

(21) Frisch, M. J.; Trucks, G. W.; Schlegel, H. B.; Scuseria, M. A.; Robb, M. A.; Cheeseman, J. R.; Zakrzewski, V. G.; Montgomery, J. A.; Stratmann, R. E.; Burant, J. C.; Dapprich, S.; Milliam, J. M.; Daniels, A. D.; Kudin, K. N.; Strain, M. C.; Farkas, O.; Tomasi, J.; Barone, V.; Cossi, M.; Cammi, R.; Mennucci, B.; Pomelli, C.; Adamo, C.; Clifford, S.; Ochterski, J.; Petersson, G. A.; Ayala, P. Y.; Cui, Q.; Morokuma, K.; Malick, D. K.; Rabuck, A. D.; Raghavachari, K.; Foresman, J. B.; Cioslowski, J.; Ortiz, J. V.; Stefanow, B. B.; Liu, G.; Liashenko, A.; Piskorz, P.; Komaromi, A.; Gomperts, R.; Martin, R. L.; Fox, D. J.; Keith, T.; Al-Laham, M. A.; Peng, C. Y.; Nanayakkara, A.; Gonzalez, C.; Challacombe, M.; Gill, P. M. W.; Johnson, B. G.; Chen. W.; Wong, M. W.; Andres, J. L.; Head-Gordon, M.; Replogle, E. S.; Pople, J. A. *GAUSSIAN 98* (revision A.11); Gaussian, Inc.: Pittsburgh, PA, 1998.

(22) Basch, H.; Hoz, S. *J. Phys. Chem. A* **1997**, *101*, 4416−4431.

(23) For a review, see: Bartlett, R. J. *J. Phys. Chem.* **1989**, *93*, 1967.

(24) Raghavachari, K.; Trucks, G. W.; Pople, J. A.; Head-Gordon, M. *Chem. Phys. Lett.* **1989**, *157*, 479.

(25) Knowles, P. J.; Hampel, C.; Werner, H.-J. *J. Chem. Phys.* **1993**, *99*, 5219.

(26) (a) Purvis, G. D.; Bartlett, R. J. *J. Chem. Phys.* **1982**, *76*, 1910. (b) Hampel, C.; Peterson, K. A.; Werner, H.-J. *Chem. Phys. Lett.* **1992**, *190*, 1. (c) Deegan, M. J. O.; Knowles, P. J. *Chem. Phys. Lett.* **1994**, *227*, 321.

(27) Frisch, M. J.; Pople, J. A.; Binkley, J. S. *J. Chem. Phys.* **1984**, *80*, 3265.

(28) Hehre, W. J.; Radom, L.; Schleyer, P, v. R.; Pople, J. A. *Ab Initio Molecular Orbital Theory;* John Wiley: New York, 1986; pp 86−87.

(29) Frisch, M. J.; Pople, J. A.; Binkley, J. S. *J. Chem. Phys.* **1984**, *80*, 3265.

(30) Werner, H.-J.; Knowles, P. J.; Almlöf, J.; Amos, R. D.; Berning, A.; Cooper, D. L.; Deegan, M. J. O.; Dobbyn, A. J.; Eckert, S. T.; Hampel, C.; Leininger, C.; Lindh, R.; Lloyd, A. W.; Meyer, W.; Mura, M. E.; Nicklass, A.; Palmieri P.; Peterson, K. A.; Pitzer, R.; Pulay, P.; Rauhaut, G.; Schütz, M.; Stoll, H.; Stone, A. J.; Thorsteinsson, T. *MOLPRO*, version 98.1; University of Stuttgart, Germany, 1998.

(31) See, e.g., McQuarrie, D. *Statistical Mechanics;* Harper and Row: New York, 1986.

(32) Vereecken, L.; Peeters, P. *J. Phys. Chem. A* **1999**, *103*, 1768−1775.

(33) Knyazev, V. D.; Slagle, I. R. *J. Phys. Chem. A* **1998**, *102*, 1770.

(34) (a) Rienstra-Kiracofe, J. C.; Allen, W. D.; Schaefer, H. F., III *J. Phys. Chem. A* **2000**, *104*, 9823. (b) Ignatyev, I.; Xie, Y.; Allen, W. D.; Schaefer, H. F., III *J. Chem. Phys.* **1997**, *107*, 141. (c) Quelch, G. E.; Gallo, M. M.; Shen, M.; Xie, Y.; Schaefer, H. F., III *J. Am. Chem. Soc.* **1994**, *116*, 4953.

(35) Goddard, W. A., III; Dunning, T. H.; Hunt, W. J.; Hay, P. J. *Acc. Chem. Res.* **1973**, *6*, 368.

(36) Olivella, S.; Anglada, J. M.; Solé, A.; Bofill, J. M. *Chem. Eur. J.* **2004**, *10*, 3404−3410.

(37) Boys, S. Y.; Bernardi, F. *Mol. Phys.* **1970**, *19*, 553.

(38) van Duijneveldt, F. B.; van Duijneveldt-van de Rijdt, J. G. C. M.; Lenthe, J. H. *Chem. Rev.* **1994**, *94*, 1873.

(39) Baldwin, R. R.; Dean, D. E.; Walker, R. W. *J. Chem. Soc., Faraday Trans. 2* **1986**, *82*, 1445.

(40) For instance, at the UCCSD(T)/6-311+G(3df,2p)//B3LYP/6-31G-(d,p) level, α-hydroxyethyl radical is calculated to be 10.4 kcal/mol less energetic than ethoxy radical.

(41) Ghigo, G.; Tonachini, G. *J. Chem. Phys* **1999**, *110*, 7298−7304.